

Acoustic diamond resonators with ultra-small mode volumes

Mikołaj K. Schmidt,^{1,*} Christopher G. Poulton,² and Michael J. Steel¹

¹Macquarie University Research Centre in Quantum Engineering (MQCQE), MQ Photonics Research Centre, Department of Physics and Astronomy, Macquarie University, NSW 2109, Australia.

²School of Mathematical and Physical Sciences, University of Technology Sydney, NSW 2007, Australia.

Quantum acoustodynamics (QAD) is a rapidly developing field of research, offering possibilities to realize and study macroscopic quantum-mechanical systems in a new range of frequencies, and implement novel transducers and memories for hybrid quantum devices. Here we propose a novel design for a versatile diamond QAD cavity operating at GHz frequencies, exhibiting effective mode volumes of about $10^{-4}\lambda^3$. Our phononic crystal waveguide cavity implements a non-resonant analogue of the optical lightning-rod effect to localize the energy of an acoustic mode into a deeply-subwavelength volume. We demonstrate that this confinement can readily enhance the orbit-strain interaction with embedded nitrogen-vacancy centres towards the high-cooperativity regime, and enable efficient resonant cooling of the acoustic vibrations towards the ground state using a single NV. This architecture can be readily translated towards setups with multiple cavities in one- or two-dimensional phononic crystals, and the underlying non-resonant localization mechanism can be implemented in phoxonic crystal defects.

I. INTRODUCTION

Rapid progress towards implementing GHz phonon-mediated quantum platforms is closely mirroring the path previously tread by the integrated cavity and waveguide quantum electrodynamics. The acoustic toolbox now includes large- Q cavities relying on surface [1, 2] and bulk phonons [3], emitters of non-classical acoustic waves [4] — all of which are being optimized to increase the fidelity of control by engineering optomechanical [5] and piezoelectric interactions [6].

A natural next step towards expanding this toolbox is to engineer a more efficient coupling between the readily available, optically controllable emitters of single phonons — for example negatively charged nitrogen-vacancy defects in diamond (NV^- 's) — and acoustic resonators [7]. This strain coupling is predominantly determined by cavities' ability to spatially focus phonons beyond the Rayleigh limit $\propto \lambda^3$, and by suppressing the dissipation of phonons into radiative and non-radiative channels. These effects, quantified by the effective mode volume of the acoustic mode V_{eff} , and acoustic quality factor Q , respectively, provide a measure of cavity performance through the acoustic analogue of Purcell factor $P_F \propto Q/V_{\text{eff}}$ [8].

Analogous challenges in electrodynamics are typically addressed by optimizing either one of the characteristics determining the Purcell factor. In plasmonic systems, large $P_F \sim 10^5$ [9, 10] can be realized in systems with very small effective mode volumes $V_{\text{eff}} \sim 10^{-4}\lambda^3$, and small $Q \sim 10$ [11]. Alternatively, all-dielectric systems [12] can provide large Q through the engineering of a near-perfect-reflection on Bragg mirrors [13] or by utilizing Whispering Gallery Modes [14], but they exhibit no ability to spatially confine light below the Rayleigh

limit. Recently reported, new approaches are merging these advantages, by either utilizing hybrid plasmonic-dielectric cavities [15, 16], or implementing defects in photonic crystal waveguides (with intrinsically large Q 's) specifically engineered to strongly localize electric field (with $V_{\text{eff}} \sim 10^{-5}\lambda^3$) [17–19].

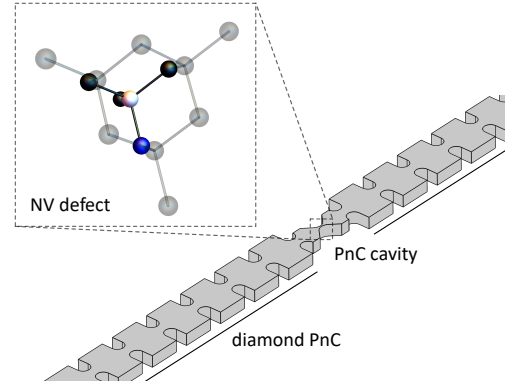


FIG. 1. Schematics of an acoustic diamond resonator with ultra-small volume mode localized at the defect (see Section II) of a finite 1D phononic waveguide (see Section III). Orbital states of the nitrogen-vacancy defect (NV^-) are coupled to the strain of the mode via parametric or resonant interaction (see Section V)

In this work, we translate this last concept into the acoustic domain, by designing sub-wavelength defects in diamond phononic crystal waveguides (PnCW), schematically shown in Fig. 1. The central defect localizes the strain through an acoustic analogue of the lightning-rod effect [20], confining the energy of the acoustic mode into effective volumes a few orders of magnitude below their bulk extent. As we show below, a significant localization characterized with $V_{\text{eff}} \sim 10^{-4}\lambda^3$ can be achieved in state-of-the-art diamond waveguides. This leads to a significant amplification of the coupling between phonon

* mikolaj.schmidt@mq.edu.au

emitters in diamond (e.g. orbital states of NVs), and mechanical modes of the structure, opening pathways to implementing high-cooperativity NV-phonon coupling on the nanoscale. In particular, we estimate that in our systems the cooperativities of both the resonant and parametric couplings, which we describe in more detail, can be enhanced to $C_{E_1} \sim 8$ and $C_{E_2} \sim 0.7$.

The paper is structured as follows: in Sections II and III we introduce two key elements of our design — mechanisms of strain localization in ultra-small mode volumes, and designs of crystal waveguides with complete acoustic bandgaps. In Section IV we assemble these two elements into Phononic Crystal Waveguide (PnC) cavities, and provide estimates for their effective mode volumes. Finally, in Section V we discuss two mechanisms of coupling between the intrinsic strain fields of the acoustic modes and the orbital states of the NV centers, calculate the coupling strengths, resulting cooperativities, and efficiencies of the the resonant and off-resonant cooling protocols [21–24].

II. CAVITY DESIGN

Let us consider a modal picture of the elastic response of an arbitrary mechanical resonator. The confinement of a particular elastic mode indexed as α in the resonator can be qualitatively expressed through an effective volume $V_{\text{eff},\alpha}$ which, neglecting the spectral dispersion and losses in the acoustic response of the materials, can be defined as [25]

$$V_{\text{eff},\alpha} = \frac{\int d\mathbf{r} h(\mathbf{r}; \alpha)}{\max h(\mathbf{r}; \alpha)}, \quad (1)$$

where the local energy density $h(\mathbf{r}; \alpha)$, averaged over the acoustic period $2\pi/\omega_\alpha$, is given as a sum of the kinetic and strain energy densities:

$$h(\mathbf{r}; \alpha) = \frac{1}{2} \bar{\epsilon}_\alpha(\mathbf{r})^* : \tilde{c}(\mathbf{r}) : \bar{\epsilon}_\alpha(\mathbf{r}) + \frac{1}{2} \omega_\alpha^2 \rho(\mathbf{r}) |\mathbf{u}_\alpha(\mathbf{r})|^2. \quad (2)$$

The mode is characterized by the displacement field \mathbf{u}_α , strain tensor $\bar{\epsilon}_\alpha = \nabla_S \mathbf{u}_\alpha$, and ρ and \tilde{c} are the local density and the 4-th rank stiffness tensor, respectively. When integrated over the volume of the resonator, the two terms in Eq. (2) yield equal contributions to the total energy. However, we should note that this equivalence does not hold locally.

From the definition of the effective mode volume, we find that $V_{\text{eff},\alpha}$ can be reduced by locally boosting energy density h . Notably, this local enhancement does not have to originate from any resonant phenomena, and — within the approximation of dispersionless material properties — can be inferred from static analysis. One such static mechanism is the acoustic analogue of the lightning-rod effect, where the strain is localized in a tapered, sub-wavelength bridge structure shown schematically in Fig. 2(b). To access some fundamental characteristics of this mechanism, we can consider a simplified 2D

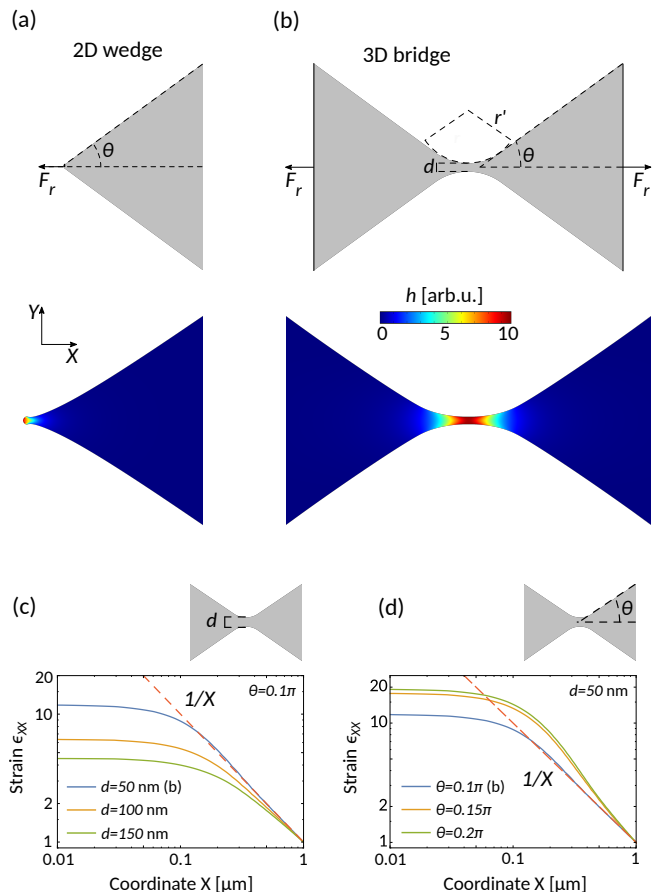


FIG. 2. Mechanism of non-resonant strain localization in a (a) truncated 2D wedge and (b) 3D bridge. The two structures, with geometries depicted with gray schematics, are deformed in the lower panels according to the displacement field, and colored to indicate energy density distribution $h(\mathbf{r}; \alpha)$. The deformations are exaggerated for illustrative purposes. (c,d) Dependence of the axial strain on parameters of the bridge marked schematically in (b): bridge thickness d and opening angle θ calculated along the symmetry axis X (dashed horizontal line at $Y = 0$). Red dashed line represents X^{-1} strain decay found for a 2D wedge, indicative of the acoustic analogue of the lightning rod effect. The bridge is engineered in the slab of thickness $h_t = 0.5 \mu\text{m}$ used throughout this work, and the curvature is set to $r' = 0.6 \mu\text{m}$.

system, with the tapered semi-infinite wedge shown in Fig. 2(a). When an axial force $\mathbf{F}_r = F_r \hat{X}$ (with $F_r < 0$) is applied to its tip, the strain is localized and exhibits a r^{-1} divergence [26]:

$$\varepsilon_{rr}(r, \phi) = -\frac{F_r}{E} \frac{\cos \phi}{r \left[\theta - \frac{1}{2} \sin(2\theta) \right]}, \quad (3)$$

$$\varepsilon_{\phi r}(r, \phi) = \varepsilon_{\phi\phi}(r, \phi) = 0, \quad (4)$$

where r ($r = 0$ at the tip) and ϕ are the polar coordinates, and E is the Young's modulus of the material. Here we approximate the diamond as an isotropic medium

with $E = 1050$ GPa, Poisson ratio of 0.2 and density of 3500 kg/m³ [27]. Energy density and displacement shown in Fig. 2(a) were calculated using COMSOL software assuming a finite tip thickness to ensure that the problem is well-posed, and therefore yield finite localization near the tip.

Building on this phenomenon of a lightning-rod-like behavior, we consider the tapered bridge as a symmetric, 3D finite-width extension of the tip setup with thickness (along the out-of-plane axis Z) $h_t = 0.5$ μm , and expect a similar localization of the axial strain at the center of the bridge (see Fig. 2(b)). To illustrate this effect quantitatively, in Fig. 2(c,d) we plot the axial (XX) component of the strain fields along the axis of the bridge (where polar coordinate r becomes X) for a range of (c) bridge widths d and (d) tapering angles θ . All the values in plots are normalized to the strain at $X = 1$ μm for clarity. We find that the largest localization of strain is offered by the narrowest bridges, and larger wedge angles θ — this latter behavior being a deviation from the one-sided analytical system. In agreement with the analytical model of a one-sided wedge, the strain exhibits a X^{-1} decay away from the bridge, and becomes effectively homogeneous inside the bridge structure. We can therefore estimate that the mode is localized in the 2D plane to an approximate area of the bridge $r'd$, or in 3D to its volume $h_t r'd$.

Local strain could be further amplified (and effective surface and volume — reduced) if we considered an even narrower bridge, or a smaller curvature radius r' . However, we impose lower limitations on d corresponding to the state of the art of lithography techniques in diamond [28], where the smallest reliably fabricated features are about 50 nm. Simultaneously, we keep the curvature r' — which determines the length of the bridge — larger, to accommodate multiple NVs which would be homogeneously coupled to the cavity mode. We briefly discuss the collective effects in Appendix B.

III. QUASI-1D PHONONIC CRYSTAL

While the acoustic lightning-rod effect provides a mechanism for non-resonant sub-wavelength localization of the strain field, the modal properties of the cavity in a phononic crystal waveguide — its frequency and quality factor — are determined by the reflection from the acoustic crystal waveguide structure (Fig. 1), and the larger-scale structure of the cavity.

In Fig. 3(a) we present a design for a unit cell of a 1D phononic crystal waveguide based on the designs widely used for a 2D phononic shield in silicon [29, 30], and — more recently — in diamond [24]. The geometric parameters shown Fig. 3(a) — in particular, the width of the connecting bridge B — governs the bandgap of the structure along the X direction. By choosing $(A, B, R) = (1.925, 0.2, 0.29)$ μm , we engineer the dispersion relation of the Z -symmetric and Z -antisymmetric modes (shown with blue and orange lines in Fig. 3(b)) to

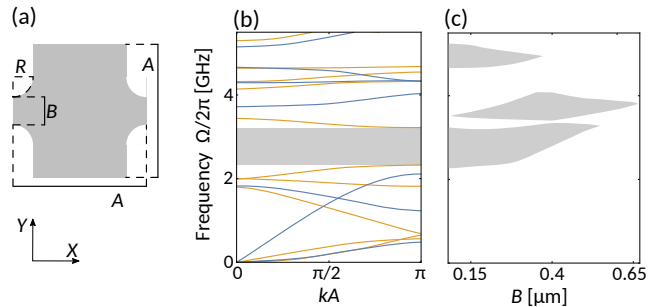


FIG. 3. Engineering a quasi-1D phonon crystal in a $h_t = 0.5$ μm thick slab of diamond. (a) Geometry of a unit cell with parameters given in the text. (b) Phononic dispersion with Z -symmetric (understood as u_Z component of the displacement field being symmetric with respect to the Z plane symmetry; blue lines) and Z -antisymmetric (orange lines) branches exhibits a broad complete acoustic bandgap (shaded region), which can be (c) tuned or closed by changing the width of the connecting structures B . Geometric parameters are given in the text.

exhibit a complete bandgap between 2.3 and 3.2 GHz. All the results were obtained with COMSOL software package [31] by implementing Floquet boundary conditions along the axis of the unit cell.

We should also note that, unlike in photonic crystal waveguide cavities, acoustic cavities can be engineered as a single defect in a phononic crystal waveguide with a complete bandgap, without any adiabatic transition region between the defect and the Bragg mirrors. This is because phonons emitted from the cavity cannot efficiently outcouple into free radiation in the surrounding medium, and the changes to the phonon momentum at the interface between the cavity and the acoustic Bragg mirror can be arbitrarily large. Therefore, using the designs of unit cell given in Fig. 3(a), we can proceed to interface the Bragg structure directly with the defect cavity, and estimate the effective volumes and quality factors of the resulting cavity modes.

IV. PHONONIC CRYSTAL WAVEGUIDE CAVITY

In Fig. 4(a) we present the design and characteristics of the entire PnC cavity. The dimensions of the bridge structure in the cavity (its width d , curvature radius r' and opening angle θ ; see (b)) determine the localization of elastic strain energy, and the auxiliary parameters b and c govern the frequency of the cavity mode. When this frequency matches the bandgap of the quasi-1D crystal, radiative phonon dissipation is suppressed. In particular, in panel (e) we show the confinement of the mode tuned to the centre of the bandgap (parameters are given in the caption) with $\Omega_\alpha/2\pi = 2.8$ GHz mode with 4 unit cells of the phononic crystal on each side of the cavity, for which we estimate the radiative losses to limit the acous-

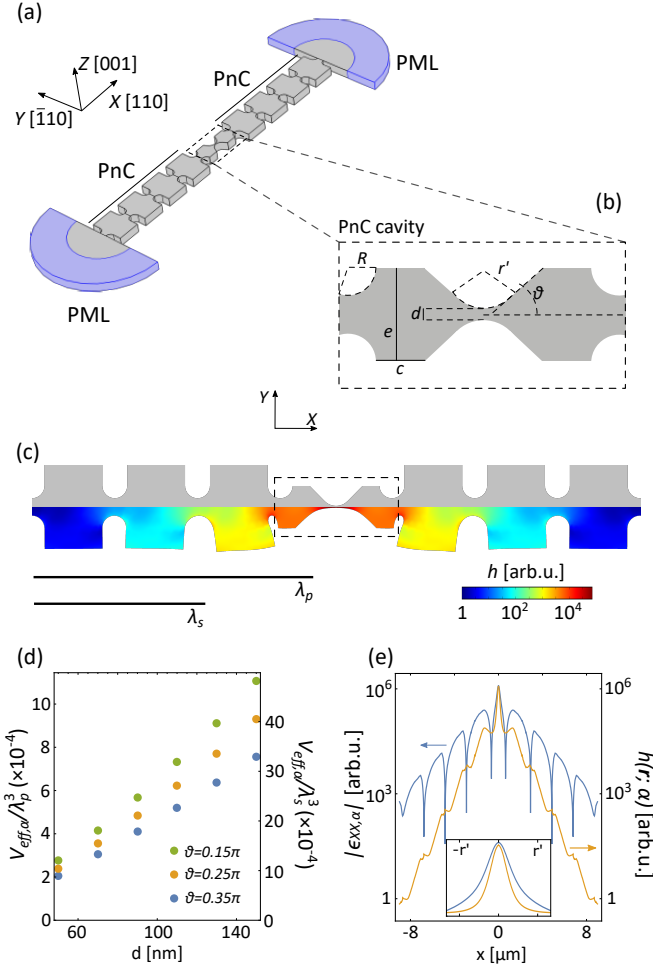


FIG. 4. Design and characteristics of the PnCW cavity. (a) Complete design of the cavity and anchoring to the substrate (colored regions denoting Perfectly Matching Layers (PML)), with the (b) magnified region showing the geometry of the interface between the defect and a unit cell of the 1D phononic crystal. In (c), as in Fig. 2, we show the displacement field of the cavity mode and energy density distribution $h(\mathbf{r}; \alpha)$, calculated for $(d, c, e, r') = (50, 400, 960, 375)$ nm and $\theta = 0.15\pi$. Bars underneath denote P and S elastic wavelengths in diamond at the mode frequency $\Omega_\alpha/2\pi = 2.8$ GHz. (d) Dependence of the effective mode volume $V_{\text{eff},\alpha}$, normalized by the wavelength of the P wave diamond, on the thickness of the cavity bridge d and opening angle θ . (e) Energy density and strain $|\varepsilon_{XX,\alpha}|$ amplitude along the axis of the crystal demonstrates the exponential localization of the mode to the cavity. Inset shows the distribution of $|\varepsilon_{XX,\alpha}|$ and $h(\mathbf{r}; \alpha)$ in the central part of the cavity.

tic quality factor $Q \sim 10^6$. For this structure, we find the effective mode volumes $V_{\text{eff},\alpha}$ of the order of $10^{-4}\lambda_p^3$, or $10^{-3}\lambda_s^3$, where λ_p and λ_s are the longitudinal and shear wavelengths of elastic wave in bulk diamond at the frequency of the mode.

In these calculations, the only mechanisms limiting the mechanical quality factor Q are related to the radiative

dissipation and clamping losses, while contributions from intrinsic mechanisms are neglected. We briefly discuss the state of the art of crystal cavity fabrication in diamond, and methods of mitigating these limitations, in Section VI. Furthermore, throughout the rest of the paper, we take a more conservative estimate of the mechanical quality factor $Q = 10^5$.

V. ORBITAL STATES OF NV AND COUPLING TO THE STRAIN

We now consider a coupling between a phonon emitter — in this case, a negatively charged NV^- center positioned at the center of the cavity — and the strain field of the acoustic cavity mode, due to the modification of the Coulomb interaction between ions of the lattice induced by acoustic vibrations [32]. This interaction is in a good approximation linear in strain, and can be thus written in a general form as

$$H_{\text{strain-NV}} = \sum_{ij \in \{x,y,z\}} V_{ij} \epsilon_{ij}, \quad (5)$$

where V_{ij} are operators describing transitions between states of the NV^- , and ϵ_{ij} is the strain tensors. This expression can be simplified by a projection onto the irreducible representation $\Gamma \in \{A_1, A_2, E\}$ of the C_{3v} symmetric group of the NV (depicted schematically in Fig. 5(a)) [33, 34]. This projection separates the contributions from three terms interactions denoted schematically in Fig. 5(a,b) [7]:

$$H_{\text{strain-NV}} = H_A + H_{E_1} + H_{E_2}. \quad (6)$$

Here we consider the orbital states $|x\rangle$ and $|y\rangle$ within the excited 3E , $m_s = 0$ manifold of the NV^- , which exhibit much stronger strain-orbit coupling than those in the ground state A_2 [7]. The orbital states are defined in the local coordinate system of the NV, where axis z is chosen along the N-V bond (aligned with $[\bar{1}\bar{1}\bar{1}]$, $[11\bar{1}]$, $[\bar{1}11]$, or $[1\bar{1}1]$), and axis x is determined by the projection of either one of the three vacancy-carbon bonds onto plane perpendicular to z . In this basis, the first two terms in Hamiltonian $H_{\text{strain-NV}}$ represent parametric couplings that shift and split the orbital states $|x\rangle$ and $|y\rangle$, while the last one resonantly couples them to the strain field. In the following subsections we discuss the latter two in more detail, estimate the cooperativities of the two couplings and the feasibility of realizing two phonon cooling protocols based on the parametric and resonant interactions [7, 21, 35]. Finally, we should note that the energy level schematic in Fig. 5(b) represents shifting of levels resulting from the interaction with a *static* strain, while the parametric interaction with *dynamic* acoustic field results in the formation of sidebands, detuned from the energies of the bare orbital states $|x\rangle$ and $|y\rangle$ by the acoustic frequency Ω_α .

To provide an estimation of the coupling between the transitions in the NV and phonon modes, we need to

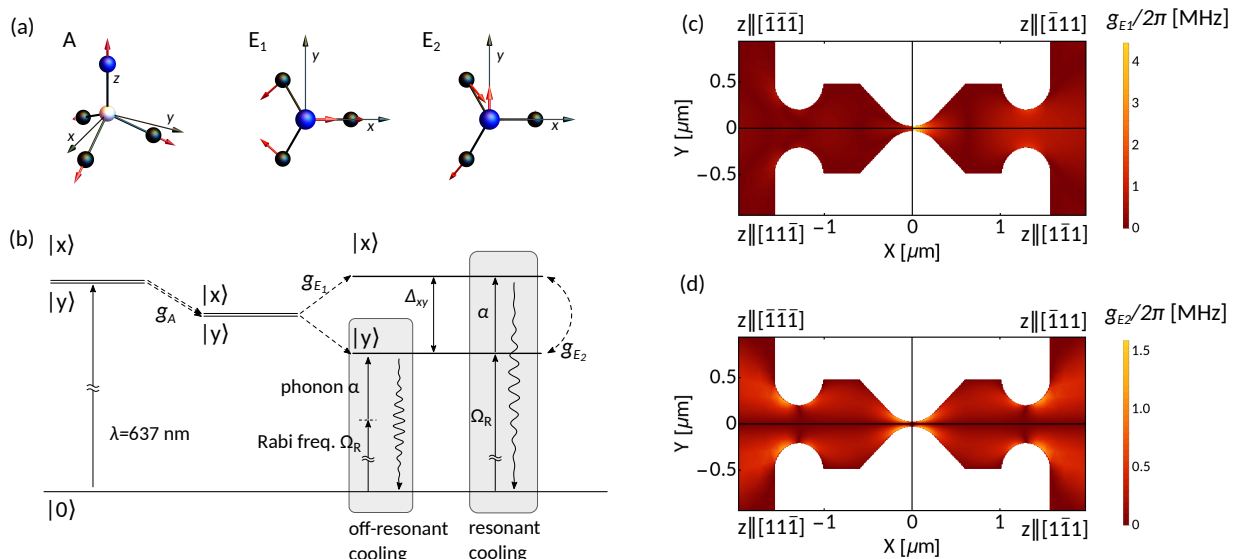


FIG. 5. Coupling between orbital states of the NV and strain field. (a) Displacements of carbon (black) and nitrogen (blue) atoms associated with A_1 , E_1 and E_2 irreducible representations of the crystal strain. (b) Energy structure of the $m_s = 0$ manifold of NV defects in diamond and effects of coupling with the crystal strain, as discussed in the text. Two cooling protocols proposed by Kepesidis *et al.* [21], involving optical driving of the excited states with Rabi frequency Ω_R , and engineering coupling with GHz phonons in mode α , are schematically shown in shaded rectangles. (c,d) Position-dependent coupling parameters (c) g_{E_1} and (d) g_{E_2} calculated for NV centers 5 nm below the surface of the diamond, with different orientations of the NV coordinate system (orientation of the z axis is given in the corners by Miller indices).

introduce a quantized picture of the elastic vibrations and then consider the exact form of coupling between the NVs and the mode of the resonator. The quantization of the elastic field can be carried out following the scheme previously explored for optical subwavelength lossless resonators with inhomogeneous field distribution [36]. We outline this procedure in Appendix A, and arrive at the quantum operators corresponding to the displacement field $\hat{\mathbf{u}}_\alpha$ and strain tensor $\hat{\hat{\varepsilon}}_\alpha$, the latter of which takes on the following form:

$$\hat{\hat{\varepsilon}}_\alpha(\mathbf{r}) = \sqrt{\frac{\hbar}{2\Omega_\alpha}} \left\{ \bar{\varepsilon}_\alpha(\mathbf{r}) b_\alpha + [\bar{\varepsilon}_\alpha(\mathbf{r})]^* b_\alpha^\dagger \right\}. \quad (7)$$

In the above definition, the classical strain tensor ε_α is normalized as $\Omega_\alpha^{-2} \int \bar{\varepsilon}_\alpha(\mathbf{r}) : \check{\varepsilon}(\mathbf{r}) : \bar{\varepsilon}_\alpha(\mathbf{r}) d\mathbf{r} = 1$, and phonon annihilation and creation operators b_α and b_α^\dagger follow the bosonic commutation relations $[b_\alpha, b_{\alpha'}^\dagger] = \delta_{\alpha, \alpha'}$.

We should note that the above quantization procedure is not exact for any realistic system with non-vanishing radiative dissipation of the acoustic waves. Similarly as in the case of photonic crystals or scattering particles, the integral given in Eq. (1) diverges as the integration volume is increased due to the radiative component of the fields, and we should embrace the picture of acoustic analogues of the quasi-normal modes [37, 38]. However, for high-Q modes discussed here the corrections to the coupling parameters or the quality factors should be negligible.

While the elastic response of the diamond, which we have assumed to be isotropic, is independent of its crystallographic orientation, the coupling between acoustic modes and NVs will strongly depend on their mutual orientation. As in the reported experimental realizations of diamond waveguides [22], we assume that the crystal coordinate system (X, Y, Z) is chosen so that $X \parallel [110]$, $Y \parallel [\bar{1}10]$, $Z \parallel [001]$ (see Fig. 4). NVs can take on 4 orientations, which are not expected to exhibit degenerate coupling identified earlier in cantilever resonators [22], and each one has to be analyzed separately.

A. Parametric coupling (E_1)

We first consider the parametric coupling between the excited orbital states of the NV and the strain field. This interaction, which lifts the degeneracy between the orbital states, is described by the effective Hamiltonian

$$H_{E_1} = [\lambda_E(\hat{\varepsilon}_{yy} - \hat{\varepsilon}_{xx}) + \lambda_{E'}(\hat{\varepsilon}_{xz} + \hat{\varepsilon}_{zx})] (|x\rangle\langle x| - |y\rangle\langle y|), \quad (8)$$

where all the strain tensor elements are taken at \mathbf{r}_{NV} the position of the NV centre, and in the local coordinate system determined by the orientation of the NV. λ_E , $\lambda_{E'}$ are strain susceptibilities or orbital-strain-constants of the NV, taken as $\lambda_E = -0.85$ PHz and $\lambda_{E'} = 0.02$ PHz [22]. Using the quantum-mechanical picture of the elastic modes in the cavity, we can rewrite it in terms of the ef-

fective strain-orbit coupling with coupling coefficient g_{E_1} :

$$H_{E_1} = g_{E_1} (b + b^\dagger) (|x\rangle \langle x| - |y\rangle \langle y|), \quad (9)$$

with $g_{E_1} = \sqrt{\hbar/2\Omega_\alpha} \{ \lambda_E [\varepsilon_{\alpha,yy}(\mathbf{r}_{\text{NV}}) - \varepsilon_{\alpha,xx}(\mathbf{r}_{\text{NV}})] + \lambda_{E'} [\varepsilon_{\alpha,xz}(\mathbf{r}_{\text{NV}}) + \varepsilon_{\alpha,zx}(\mathbf{r}_{\text{NV}})] \}$. Since $\lambda_E \gg \lambda_{E'}$ [22], the coupling term will be dominated by the diagonal elements of the strain tensor $\varepsilon_{\alpha,xx}$ and $\varepsilon_{\alpha,yy}$, and therefore by the longitudinal components of the strain.

In the map of g_{E_1} in Fig. 5(c) we consider separately four orientations of the NV, defined by the z (x) axes along the $[\bar{1}\bar{1}\bar{1}]$ ($[11\bar{2}]$), $[11\bar{1}]$ ($[\bar{1}\bar{1}\bar{2}]$), $[\bar{1}11]$ ($[1\bar{1}2]$), or $[1\bar{1}\bar{1}]$ ($[\bar{1}\bar{1}2]$) directions, in a plane 5 nm below the upper surface of the diamond. Such shallow defects can be generated using low-energy ion implantation [39]. However, we should note that unlike the Surface Acoustic Waves, or in the *flapping* modes of a PnCW [40] (see discussion in Section V C), our cavity exhibits an approximately constant strain along its depth (Z axis), and the exact positioning of the NV can be optimised to shield the defect from external electric fields or surface strain.

The calculated value of coupling g_{E_1} becomes more meaningful if we compare it to the dephasing rates of the involved electronic states $\Gamma_{x/y}$ ($\Gamma_{x/y}/2\pi \approx 15$ MHz [41]), and the re-thermalization rate of cavity phonons $\gamma_{\text{th}} = n_{\text{th}}\Omega_\alpha/(2Q)$ (with $n_{\text{th}} = [\exp(\hbar\Omega_\alpha/k_B T) - 1]^{-1}$). For the calculations carried out in this section, we consider resonators with slightly lower, more realistic mechanical quality $Q = 10^5$, operating at temperature of 4 K (where $n_{\text{th}}(\Omega_\alpha/2\pi = 2.4$ GHz) ≈ 35). We can then calculate the parametric coupling cooperativity $C_{E_1} = 4g_{E_1}^2/(\gamma_{\text{th}}\Gamma_{x/y})$ for the maximum coupling $g_{E_1}/2\pi = 5$ MHz as reaching $C_{E_1} \approx 8$.

Potentially, parametric coupling offers also a pathway to implementing an off-resonant phonon cooling protocol, as proposed by Wilson-Rae *et al.* in Ref. [35] (see Fig. 5(b) for a schematic of the protocol), in which the optically driven orbital states in NVs act as structured reservoirs into which the phonons would decay. By optically driving the $\omega_y - \Omega$ red sideband of the lower energy state $|y\rangle$ with Rabi frequency Ω_R (here we put $\Omega_R/2\pi = 15$ MHz = $\Gamma_{x/y}/2\pi$ to saturate the electronic states [21]), we cool the acoustic mode α at a rate [21] $\Gamma_{E_1} = g_{E_1}^2 \Omega_R^2 / (\Gamma_{x/y} \Omega_\alpha^2) \approx 400$ Hz $\ll \gamma_{\text{th}}$. This estimation indicates that the off-resonant scheme cannot efficiently cool the mechanical vibrations of the resonator. A similar conclusion was found for a submicron, high-Q acoustic cantilever resonator hypothesized by Kepesidis *et al.* [21].

B. Resonant coupling (E_2)

In the Hamiltonian given in Eq. (6), the only term describing resonant transitions between excited orbital states $|x\rangle$ and $|y\rangle$ is associated with the E_2 symmetry of the strain and reads

$$H_{E_2} = [\lambda_E (\hat{\varepsilon}_{xy} + \hat{\varepsilon}_{yx}) + \lambda_{E'} (\hat{\varepsilon}_{yz} + \hat{\varepsilon}_{zy})] (|x\rangle \langle y| + |y\rangle \langle x|). \quad (10)$$

As above, we can write down the quantized version of this interaction

$$H_{E_2} = g_{E_2} (|x\rangle \langle y| + |y\rangle \langle x|) (b^\dagger + b), \quad (11)$$

finding $g_{E_2} = \sqrt{\hbar/2\Omega_\alpha} [\lambda_E (\varepsilon_{\alpha,xy} + \varepsilon_{\alpha,yx}) + \lambda_{E'} (\varepsilon_{\alpha,yz} + \varepsilon_{\alpha,zy})]$.

Values of the g_{E_2} coupling are shown in Fig. 5(b) for the four NV orientations. Unlike in the case of the parametric interaction, the maximum coupling is not found for the emitter placed in the narrowest part of the bridge, but rather near its edges. This is because g_{E_2} depends predominantly on the off-diagonal components of the strain tensor $\varepsilon_{\alpha,xy} = \varepsilon_{\alpha,yx}$. Using the parameters defined earlier, we can estimate that the maximum coupling g_{E_2} found in our system ($g_{E_2}/2\pi \approx 1.5$ MHz) can reach near-unity cooperativity $C_{E_2} = 4g_{E_2}^2/(\gamma_{\text{th}}\Gamma_{x/y}) \approx 0.7$.

This coupling also offers a much more efficient pathway to implement cooling of the acoustic resonator by tuning the mode energy to the energy splitting between the orbital states $|x\rangle$ and $|y\rangle$ [21]. Then, optically driving the lower-laying $|y\rangle$ state with Rabi frequency Ω_R , we cool the system at rate $\Gamma_{E_2} = 4g_{E_2}^2 \Omega_R^2 / \Gamma_{x/y}^3$ [21], to a final population given approximately by $n_{\text{fin}} = \gamma_{\text{th}}/\Gamma_{E_2} \approx 1.5$ for $g_{E_2}/2\pi = 1.5$ MHz.

C. Enhancing SiV spin-phonon coupling in subwavelength cavities from Burek *et al.*

A similar problem of engineering coherent coupling between acoustic mode of a PnCW cavity and another widely analyzed colour defect in diamond — silicon vacancy (SiV) — was investigated by Meesala *et al.* in Ref. [40]. SiVs are an attractive alternative to NVs for both information storage, and spin-orbit coupling, since thanks to the strong spin-orbit coupling, spin states within the ground electronic state manifold of SiV exhibit simultaneous lower dephasing rate (of about $\Gamma_{\text{SiV,deph}}/2\pi \approx 4$ MHz at 4K and $2\pi \approx 100$ Hz at 100 mK [42]) and larger strain susceptibility (about 1.8 GHz) than NV. Meesala *et al.* noticed that the strain in a triangular crystal waveguide [43] can be resonantly localized to a small volume near the surface of the diamond for a *flapping* mode of the waveguide [43]. This localization supports resonant spin-phonon coupling with coupling $g_{\text{SiV}} \approx 0.8$ MHz, and cooperativity of $C_{\text{SiV}} \sim 1$ for resonators with $Q \sim 10^5$ or $Q \sim 10^3$, at 4K and 100 mK temperatures, respectively. This brief analysis indicates that the localization of the strain field found in structured developed by Burek *et al.* [43] yields effective mode volumes $V_{\text{eff}} \sim 10^{-3} \lambda_p^3$, comparable to those reported here, albeit achieved by a very different, nonresonant effect.

Finally, we note that by replacing NV with SiV in our cavities, and focusing on the resonant spin-phonon interaction, we could reach the cooperativities $C_{\text{SiV}} \sim 4g_{\text{SiV}}^2/(\Gamma_{\text{SiV,deph}}\kappa_b) \approx 110$, where we took $g_{\text{SiV}} = 2g_{E_2} \approx 2\pi \times 3$ MHz (to reflect the larger strain susceptibility of SiV), for 4 K temperature and ~ 8000 for 100 mK.

VI. FABRICATION CONSIDERATIONS

Maximum values of the cooperativities depend critically on the dissipation rate, or quality factor of the acoustic cavity mode. To date, to the authors' best knowledge, the maximum $Q_m \sim 7000$ was reported by Burek *et al.* [43] for few-GHz PnC cavities fabricated in bulk etched single-crystalline diamond. In a recent contribution by Cady *et al.* [24], authors reported on fabrication of diamond PnC cavities using the diamond-on-insulator technique with $Q_m \sim 100$, pointing to the significant losses induced by a leftover substrate. Both of these reports cite quality factors measured at a room temperature, and should be readily further amplified in cryogenic environment. Possible improvements could also be achieved by embracing the recently developed concepts of the soft-clamping [44] and strain engineering [45]. Furthermore, in materials for which fabrication techniques are much more matured, like silicon, much higher quality factors of PnC resonators up to 10^{10} were reported recently [5], suggesting that GHz acoustic vibrations can be used as quantum memories [46] rather than transducers [2].

VII. CONCLUSIONS

In summary, we propose a simple design of an acoustic cavity capable of localizing GHz mechanical modes into

ultrasmall volumes of about $10^{-4}\lambda_p^3$. Since these cavities are implemented as defects in quasi-one-dimensional phononic crystals, and the localization mechanism is non-resonant, the cavity frequencies can be readily tuned across the few-GHz range by changing its geometric parameters, and the quality factor is determined by the efficiency of suppression of transmission in the phononic Bragg mirrors.

We further find that such state-of-the-art cavities should, thanks to the significant spatial and spectral confinement of the acoustic mode, offer an attractive platform for implementing efficient coherent control over states of the atomic defects in diamond (NV or SiV) susceptible to the external strain. In particular, for the designs analyzed here, the resonant NV-phonon coupling operates in the high-cooperativity regime, opening a pathway to an efficient ground state resonant cooling of the cavity mode by a single NV. We also predict that similar setups could provide large-cooperativity resonant coupling between phonons and the spin states of a SiV.

The proposed design of the cavity and strain localization mechanism can be further refined and implemented in more robust architectures, including cascaded acoustic cavities for indistinguishable phonon emission [47], and quasi-two-dimensional phononic topological crystals [48], acoustic buses for efficient transfer of a quantum state between distant emitters [27]. They should also be readily adapted to simultaneously co-localize high-Q optical mode [17–19] to enable more efficient optical control of the defects.

-
- [1] T. Aref, P. Delsing, M. K. Ekström, A. F. Kockum, M. V. Gustafsson, G. Johansson, P. J. Leek, E. Magnusson, and R. Manenti, in *Superconducting devices in quantum optics* (Springer, 2016) pp. 217–244.
 - [2] M. J. A. Schuetz, E. M. Kessler, G. Giedke, L. M. K. Vandersypen, M. D. Lukin, and J. I. Cirac, *Phys. Rev. X* **5**, 031031 (2015).
 - [3] Y. Chu, P. Kharel, T. Yoon, L. Frunzio, P. T. Rakich, and R. J. Schoelkopf, *Nature* **563**, 666 (2018).
 - [4] Y. Chu, P. Kharel, W. H. Renninger, L. D. Burkhardt, L. Frunzio, P. T. Rakich, and R. J. Schoelkopf, *Science* **358**, 199 (2017).
 - [5] G. S. MacCabe, H. Ren, J. Luo, J. D. Cohen, H. Zhou, A. Sipahigil, M. Mirhosseini, and O. Painter, arXiv preprint arXiv:1901.04129 (2019).
 - [6] P. Arrangoiz-Arriola, E. A. Wollack, M. Pechal, J. D. Witmer, J. T. Hill, and A. H. Safavi-Naeini, *Phys. Rev. X* **8**, 031007 (2018).
 - [7] D. Lee, K. W. Lee, J. V. Cady, P. Ovartchaiyapong, and A. C. B. Jayich, *J. Opt.* **19**, 033001 (2017).
 - [8] M. K. Schmidt, L. G. Helt, C. G. Poulton, and M. J. Steel, *Phys. Rev. Lett.* **121**, 064301 (2018).
 - [9] N. Kongsuwan, A. Demetriadou, R. Chikkaraddy, F. Benz, V. A. Turek, U. F. Keyser, J. J. Baumberg, and O. Hess, *Acs Photonics* **5**, 186 (2017).
 - [10] R. Chikkaraddy, B. De Nijs, F. Benz, S. J. Barrow, O. A. Scherman, E. Rosta, A. Demetriadou, P. Fox, O. Hess, and J. J. Baumberg, *Nature* **535**, 127 (2016).
 - [11] A. F. Koenderink, *ACS photonics* **4**, 710 (2017).
 - [12] P. Lodahl, S. Mahmoodian, and S. Stobbe, *Reviews of Modern Physics* **87**, 347 (2015).
 - [13] J. P. Reithmaier, G. Sek, A. Löffler, C. Hofmann, S. Kuhn, S. Reitzenstein, L. Keldysh, V. Kulakovskii, T. Reinecke, and A. Forchel, *Nature* **432**, 197 (2004).
 - [14] T. Aoki, B. Dayan, E. Wilcut, W. P. Bowen, A. S. Parkins, T. Kippenberg, K. Vahala, and H. Kimble, *Nature* **443**, 671 (2006).
 - [15] H. M. Doeleman, E. Verhagen, and A. F. Koenderink, *ACS Photonics* **3**, 1943 (2016).
 - [16] A. Bozzola, S. Perotto, and F. De Angelis, *Analyst* **142**, 883 (2017).
 - [17] S. Hu and S. M. Weiss, *ACS Photonics* **3**, 1647 (2016).
 - [18] H. Choi, M. Heuck, and D. Englund, *Phys. Rev. Lett.* **118**, 223605 (2017).
 - [19] S. Hu, M. Khater, R. Salas-Montiel, E. Kratschmer, S. Engelmann, W. M. J. Green, and S. M. Weiss, *Science Advances* **4** (2018), 10.1126/sciadv.aat2355.
 - [20] J. Van Bladel and J. Van Bladel, *Singular electromagnetic fields and sources* (Clarendon Press Oxford, 1991).
 - [21] K. V. Kepesidis, S. D. Bennett, S. Portolan, M. D. Lukin, and P. Rabl, *Phys. Rev. B* **88**, 064105 (2013).
 - [22] K. W. Lee, D. Lee, P. Ovartchaiyapong, J. Minguzzi,

- J. R. Maze, and A. C. Bleszynski Jayich, *Phys. Rev. Applied* **6**, 034005 (2016).
- [23] H. Y. Chen, E. R. MacQuarrie, and G. D. Fuchs, *Phys. Rev. Lett.* **120**, 167401 (2018).
- [24] J. V. Cady, O. Michel, K. W. Lee, R. N. Patel, C. J. Sarabalis, A. H. Safavi-Naeini, and A. C. B. Jayich, *Quantum Sci. Technol.* **4**, 024009 (2019).
- [25] M. Eichenfield, J. Chan, R. M. Camacho, K. J. Vahala, and O. Painter, *Nature* **462**, 78 (2009).
- [26] L. D. Landau and E. M. Lifshitz, *Course of Theoretical Physics Vol 7: Theory and Elasticity* (Pergamon press, 1959).
- [27] M.-A. Lemonde, S. Meesala, A. Sipahigil, M. J. A. Schuetz, M. D. Lukin, M. Loncar, and P. Rabl, *Phys. Rev. Lett.* **120**, 213603 (2018).
- [28] C. Dory, D. Vercruysee, K. Y. Yang, N. V. Sapra, A. E. Rugar, S. Sun, D. M. Lukin, A. Y. Piggott, J. L. Zhang, M. Radulaski, *et al.*, *Nat. Commun.* **10**, 1 (2019).
- [29] G. S. MacCabe, H. Ren, J. Luo, J. D. Cohen, H. Zhou, A. Sipahigil, M. Mirhosseini, and O. Painter, arXiv preprint arXiv:1901.04129 (2019).
- [30] J. Chan, A. H. Safavi-Naeini, J. T. Hill, S. Meenehan, and O. Painter, *Applied Physics Letters* **101**, 081115 (2012), <https://doi.org/10.1063/1.4747726>.
- [31] COMSOL, Inc, “COMSOL Multiphysics Reference Manual,” 4.4.
- [32] M. W. Doherty, N. B. Manson, P. Delaney, F. Jelezko, J. Wrachtrup, and L. C. Hollenberg, *Physics Reports* **528**, 1 (2013).
- [33] M. W. Doherty, N. B. Manson, P. Delaney, and L. C. Hollenberg, *New Journal of Physics* **13**, 025019 (2011).
- [34] A. Hughes and W. Runciman, *Proceedings of the Physical Society* **90**, 827 (1967).
- [35] I. Wilson-Rae, P. Zoller, and A. Imamoglu, *Phys. Rev. Lett.* **92**, 075507 (2004).
- [36] R. Esteban, J. Aizpurua, and G. W. Bryant, *New Journal of Physics* **16**, 013052 (2014).
- [37] P. T. Kristensen and S. Hughes, *ACS Photonics* **1**, 2 (2014).
- [38] C. Sauvan, J. P. Hugonin, I. S. Maksymov, and P. Lalanne, *Phys. Rev. Lett.* **110**, 237401 (2013).
- [39] J. M. Smith, S. A. Meynell, A. C. B. Jayich, and J. Meijer, *Nanophotonics* **8**, 1889 (2019).
- [40] S. Meesala, Y.-I. Sohn, B. Pingault, L. Shao, H. A. Atikian, J. Holzgrafe, M. Gündoğan, C. Stavrakas, A. Sipahigil, C. Chia, R. Evans, M. J. Burek, M. Zhang, L. Wu, J. L. Pacheco, J. Abraham, E. Bielejec, M. D. Lukin, M. Atatüre, and M. Lončar, *Phys. Rev. B* **97**, 205444 (2018).
- [41] L. Robledo, H. Bernien, I. van Weperen, and R. Hanson, *Phys. Rev. Lett.* **105**, 177403 (2010).
- [42] D. D. Sukachev, A. Sipahigil, C. T. Nguyen, M. K. Bhaskar, R. E. Evans, F. Jelezko, and M. D. Lukin, *Phys. Rev. Lett.* **119**, 223602 (2017).
- [43] M. J. Burek, J. D. Cohen, S. M. Meenehan, N. El-Sawah, C. Chia, T. Ruelle, S. Meesala, J. Rochman, H. A. Atikian, M. Markham, D. J. Twitchen, M. D. Lukin, O. Painter, and M. Lončar, *Optica* **3**, 1404 (2016).
- [44] Y. Tsaturyan, A. Barg, E. S. Polzik, and A. Schliesser, *Nature nanotechnology* **12**, 776 (2017).
- [45] A. H. Ghadimi, S. A. Fedorov, N. J. Engelsen, M. J. Beryhi, R. Schilling, D. J. Wilson, and T. J. Kippenberg, *Science* **360**, 764 (2018).
- [46] C. T. Hamm, C.-L. Zou, Y. Zhang, Y. Chu, R. J. Schoelkopf, S. M. Girvin, and L. Jiang, *Phys. Rev. Lett.* **123**, 250501 (2019).
- [47] H. Choi, D. Zhu, Y. Yoon, and D. Englund, *Phys. Rev. Lett.* **122**, 183602 (2019).
- [48] C. Brendel, V. Peano, O. Painter, and F. Marquardt, *Phys. Rev. B* **97**, 020102 (2018).
- [49] M. Reagor, W. Pfaff, C. Axline, R. W. Heeres, N. Ofek, K. Sliwa, E. Holland, C. Wang, J. Blumoff, K. Chou, M. J. Hatridge, L. Frunzio, M. H. Devoret, L. Jiang, and R. J. Schoelkopf, *Phys. Rev. B* **94**, 014506 (2016).

Appendix A: Derivation of the acoustic displacement and strain field operators

Both the displacement field $\hat{\mathbf{u}}_\alpha$ and strain tensor operators $\hat{\bar{\bar{\epsilon}}}_\alpha$ corresponding to any given mode α , should have a representation given by the classical field \mathbf{u}_α and tensor $\bar{\bar{\epsilon}}_\alpha$, respectively:

$$\hat{\bar{\bar{\epsilon}}}_\alpha(\mathbf{r}) = \sqrt{\frac{\hbar}{2\Omega_\alpha}} \left\{ \bar{\bar{\epsilon}}_\alpha(\mathbf{r})b_\alpha + [\bar{\bar{\epsilon}}_\alpha(\mathbf{r})]^* b_\alpha^\dagger \right\}. \quad (\text{A1})$$

$$\hat{\mathbf{u}}_\alpha(\mathbf{r}) = \sqrt{\frac{\hbar}{2\Omega_\alpha}} \left\{ \mathbf{u}_\alpha(\mathbf{r})b_\alpha + [\mathbf{u}_\alpha(\mathbf{r})]^* b_\alpha^\dagger \right\}. \quad (\text{A2})$$

Then the total energy of the mode can be re-written as

$$\begin{aligned} \hat{H} &= \int_V h[\hat{\bar{\bar{\epsilon}}}_\alpha(\mathbf{r})]d\mathbf{r} \\ &= \frac{\hbar}{2\Omega_\alpha} \int_V \{ b_\alpha b_\alpha^\dagger h[\bar{\bar{\epsilon}}_\alpha(\mathbf{r})] + b_\alpha^\dagger b_\alpha h[\bar{\bar{\epsilon}}_\alpha(\mathbf{r})] \} d\mathbf{r} \\ &= (2b_\alpha^\dagger b_\alpha + 1) \frac{\hbar}{2\Omega_\alpha} \int_V h[\bar{\bar{\epsilon}}_\alpha(\mathbf{r})]d\mathbf{r} = \\ &= \hbar\Omega_\alpha \left(b_\alpha^\dagger b_\alpha + \frac{1}{2} \right) \frac{1}{\Omega_\alpha^2} \int_V h[\bar{\bar{\epsilon}}_\alpha(\mathbf{r})]d\mathbf{r} \\ &= \hbar\Omega_\alpha \left(b_\alpha^\dagger b_\alpha + \frac{1}{2} \right), \end{aligned} \quad (\text{A3})$$

where in the last step we equated the derived Hamiltonian with the expected bosonic Hamiltonian, effectively defining the normalization of elastic field/strain tensor. Since the energy is equally distributed between the kinetic and strain energy components, the normalization criterion can be re-written by considering either form.

For example, by focusing on the kinetic energy, the normalization is

$$\frac{1}{\Omega_\alpha^2} \int_V h[\bar{\bar{\epsilon}}_\alpha(\mathbf{r})]d\mathbf{r} = \int_V \rho(\mathbf{r})|\mathbf{u}_\alpha(\mathbf{r})|^2 d\mathbf{r} = 1. \quad (\text{A4})$$

This is the explicit normalization used in our earlier work on elastic Purcell effect [8] with interaction between an emitter modelled as a local harmonic force and the displacement field of a resonator.

In this contribution, it is convenient to express the normalization of the strain tensor by considering the contribution from strain energy, i.e.

$$\frac{1}{\Omega_\alpha^2} \int_V h[\bar{\bar{\epsilon}}_\alpha(\mathbf{r})]d\mathbf{r} = \frac{1}{\Omega_\alpha^2} \int_V [\bar{\bar{\epsilon}}(\mathbf{r})]^* : \tilde{c}(\mathbf{r}) : \bar{\bar{\epsilon}}(\mathbf{r})d\mathbf{r} = 1. \quad (\text{A5})$$

Looking back to Eq. (1), and noting that the maximum energy density in the resonator considered in this work is determined by the maximum of strain energy, we can approximate the maximum of the norm of $\max |\bar{\bar{\epsilon}}| \approx \sqrt{\Omega_\alpha^2 / (|\tilde{c}|V_{\text{eff}})}$, yielding a crude characteristic of the coupling coefficients $g_E \sim V_{\text{eff}}^{-1/2}$. This translates to the Purcell-like enhancement of the cooperativities (both for the resonant and the parametric couplings), inversely proportional to V_{eff} .

Appendix B: Collective effects in cooling protocols

Finally, we should note that a coupling to multiple (N) NVs would provide a linear increase of the efficiency of the phonon cooling $N\Gamma_{E_1/E_2}$ for identical NVs. That is because, in the *inverse Purcell effect* (defined by the hierarchy of decay rates $\Gamma_{x/y} \gg \gamma_{\text{th}}$) [49], the NVs behave as a collection of uncorrelated reservoirs for the cavity phonons.

Furthermore, as long as the NVs are positioned near the very centre of the cavity with a constant density ρ_{NV} , and their couplings can be approximately considered as identical, any reduction or increase of the mode volume $V_{\text{eff},\alpha} \propto 1/\sqrt{g_{E_i}} \propto 1/\Gamma_{E_i}$ would not impact the cooling rate as $\Gamma_{E_i} \sim \rho V_{\text{eff},\alpha}$.